Acta Polytechnica CTU Proceedings **55**:25–32, 2025
https://doi.org/10.14311/APP.2025.55.0025

Published by the Czech Technical University in Prague

IMPACT OF FECRAL OXIDE COMPOSITION ON SEVERE ACCIDENT PROGRESSION IN MELCOR

Lukáš Hamřík[a,*], Peter Mičian[a], Štěpán Foral[a,b], Karel Katovský[a], Pavel Máca[a], Jitka Vojáčková[a]

[a] *Brno University of Technology, Faculty of Electrical Engineering and Communication, Department of Electrical Power Engineering, Technická 3058/10, 616 00 Brno, Czech Republic*

[b] *TES s.r.o., Pražská 597, 674 01 Třebíč, Czech Republic*

[*] corresponding author: Lukas.Hamrik@vutbr.cz

Abstract. Experimental studies have shown that the composition of the oxide layer forming on FeCrAl surface depends strongly on the temperature of the environment, with varying fractions of aluminum, chromium, and iron oxides forming under different conditions.

In this work, multiple oxide compositions were incorporated into MELCOR simulations for evaluation of their impact on cladding degradation. The weight fractions of aluminum, chromium, and iron oxides were derived from published experimental data, serving as basis for modifications of the material model.

Simulations of a representative Loss of Coolant Accident scenario show that these changes significantly affect cladding temperature evolution, oxidation progression, and hydrogen generation. These results highlight the need to account for environmentally dependent behavior when modeling advanced cladding materials in integral codes.

Keywords: ATF cladding, FeCrAl, LOCA, severe accident, MELCOR.

1. Introduction

The accident at the Fukushima Daiichi nuclear power plant in 2011 renewed global attention on the need for enhanced safety in nuclear power systems. In response, the nuclear industry and research community have accelerated efforts to develop advanced fuels to improve performance under accident conditions. These efforts have led to the investigation of Accident Tolerant Fuel (ATF), which may increase the resilience of nuclear fuel during severe accident scenarios while maintaining or improving overall fuel reliability and economics.

One of the promising candidates for ATF cladding materials is FeCrAl (iron-chromium-aluminum) alloy, which offers improved oxidation resistance, mechanical strength at high temperatures, and reduced hydrogen generation compared to conventional Zircaloy cladding. An important feature of FeCrAl is the formation of a protective oxide layer that significantly slows down high-temperature oxidation. However, previous MELCOR simulations that assessed FeCrAl cladding behavior during accident scenarios [1–3] have often assumed a fixed oxide composition, typically weighted in the same proportion as the base alloy. This assumption simplified the oxidation behavior, as experimental studies [4] have shown that the oxide layer composition of FeCrAl alloys varies significantly with temperature and exposure conditions.

The operation of LWR with FeCrAl cladding is not without drawbacks. FeCrAl alloys exhibit a thermal neutron absorption cross section approximately 12 times higher than that of zirconium alloys, negatively affecting the neutron economy. Performed study [5] suggest that to maintain the neutron balance compared to the Zr alloys, the FeCrAl cladding thickness needs to be reduced. Thinner cladding would allow for a slightly larger pellet diameter, however, it appears that the enrichment over 5 % would become necessary. Increased size of pellets and higher enrichment would lead to higher fuel fabrication costs.

FeCrAl cladding is currently in an advanced stage of development, with several lead test rods already irradiated in commercial LWRs under U.S. DOE programs, although full commercial deployment remains pending. In the broader context of accident-tolerant fuels, FeCrAl is still regarded as an innovative mid-term solution rather than an immediately deployable technology [6].

This study investigates how variations in the composition of FeCrAl oxide affect the progression of severe accidents. The hypothesis is that temperature-dependent changes in oxide composition significantly influence accident behavior and should be accounted for in the simulation models used in a severe accident codes.

The study utilizes the APR1400 (Advanced Power Reactor 1 400 MWe) as the reference plant model. Developed in South Korea as a Generation III pressurized water reactor, the APR1400 builds upon the design experience of the OPR1000 and incorporates advanced features for improved safety and performance. The reactor delivers a thermal output of 4 000 MW and an electrical output of 1 400 MW. Its reactor coolant

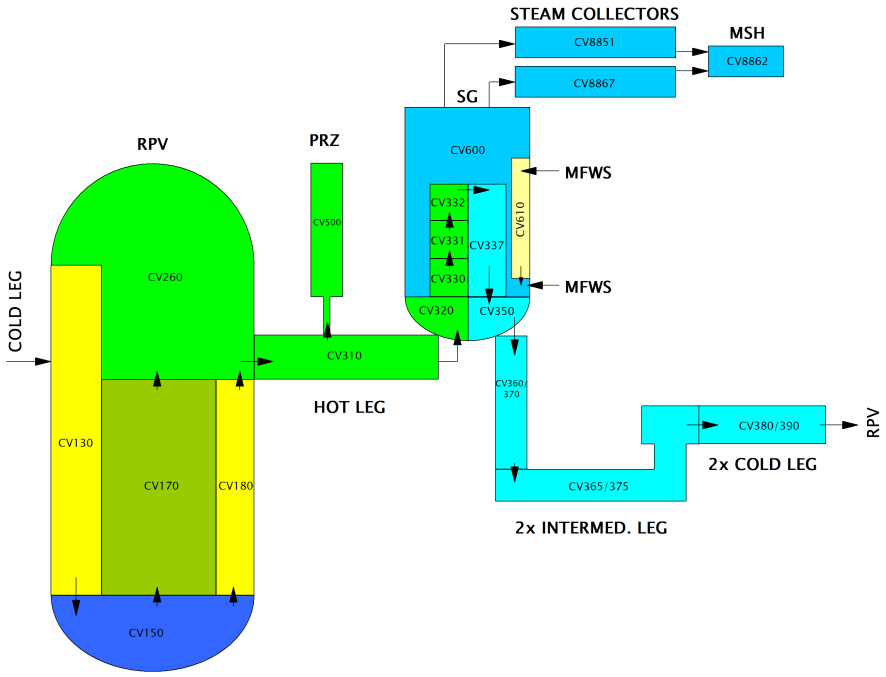

Figure 1. Part of primary and secondary loop nodalization.

system is arranged into two loops, each equipped with a steam generator and two reactor coolant pumps, resulting in a total of two hot legs and four cold legs.

2. Modeling and methods

2.1. Model and scenario

Data for the modeling of APR1400 were obtained from the Design Control Document (DCD) [7], prepared by KEPCO and KHNP, which was submitted to the U.S. Nuclear Regulatory Commission (NRC) for design certification.

The primary side in the MELCOR simulation model consists of 32 control volumes, with five of these dedicated to the reactor pressure vessel. The secondary side is modeled using 11 control volumes, incorporating components such as the steam generator, turbine system, and feedwater injection as a boundary condition. A detailed nodalization diagram is shown in Figure 1.

The reactor core is represented in Figure 2, using 15 axial levels and four radial rings. The active fuel is located in axial levels 6 through 15, specifically within radial rings 1 to 3. The lower plenum is modeled with axial levels 1 through 5, and the downcomer region around the core is represented by radial ring 4, covering axial levels 5 to 15.

Currently, the core is represented by a single control volume; a finer nodalization would provide greater detail and could improve the accuracy of thermal-hydraulic response and oxidation calculations during transient and accident conditions.

The model also includes several key safety systems, such as four Safety Injection Tanks (SITs), an In-Containment Refueling Water Storage Tank (IRWST)

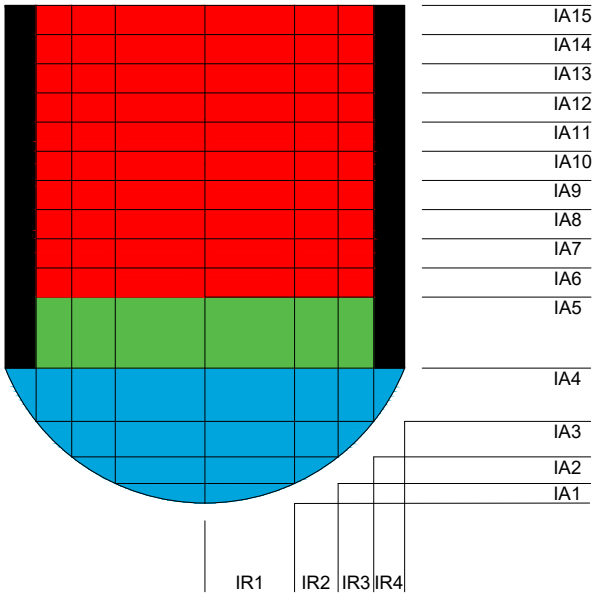

Figure 2. Core and lower plenum nodalization.

connected to four Safety Injection Pumps (SIPs), and four Pilot-Operated Safety Relief Valves (POSRVs) located at the top of the pressurizer. On the secondary side, safety mechanisms such as the Main Steam Safety Valves (MSSVs), Main Steam Isolation Valves (MSIVs), and Atmospheric Dump Valves (ADVs) are incorporated to capture system response during overpressure or isolation conditions.

The scenario analyzed in this study is a large-break loss-of-coolant accident (LB-LOCA), initiated by a guillotine break between the cold leg (CV480) and the downcomer section of the reactor pressure

Fe [wt. %]	Cr [wt. %]	Al [wt. %]	Mo [wt. %]	Si [wt. %]	Y [wt. %]
80.15	13	4.5	2	0.2	0.15

TABLE 1. FeCrAl C35M alloying elements composition.

Case	Al_2O_3 [wt. %]	Cr_2O_3 [wt. %]	Fe_3O_4 [wt. %]
Composition 1	60	5	35
Composition 2	60	10	30
Composition 3	70	5	25
Composition 4	70	10	20
Composition 5	80	5	15
Composition 6	90	5	5
Baseline (weighted with alloy composition)			

TABLE 2. Defined FeCrAl oxide compositions used in the simulations.

vessel (CV130). The break occurs in the loop without the pressurizer. The scenario assumes that only passive safety systems are available, representing an unmitigated accident progression.

For all cases, the steady state was initialized at −12 000 seconds, at time 0, the cold leg break occurred, the end of simulation time was set to 20 000 seconds. The MELCOR version used for simulations was r2024.0.0.

2.2. FeCrAl implementation and methodology

In this study, the FeCrAl C35M cladding was implemented into MELCOR using user-defined materials with temperature-dependent thermophysical properties. Properties such as thermal conductivity, specific heat capacity and enthalpy were defined as functions of temperature to reflect the behavior of advanced cladding materials under accident conditions by the data given in [8]. Reference [8] does not state the exact melting point of the C35M alloy, it was assumed that the melting point would be 1 500 °C, the same as the Kanthal APMT alloy [9]. In Table 1, the composition of the C35M alloy is shown.

Currently, the MELCOR representation of the oxide layer formed during FeCrAl oxidation is that of a single homogeneous material, as also stated in a report from Sandia National Laboratories [1]. This simplification does not allow for explicit modeling of the layered structure typically formed on the material surface which underwent oxidation in a high-temperature environment with a water contain. Consequently, a mixture-based approach was adopted, where the oxide was treated as a composite material with properties derived from the weighted contributions of the individual oxide constituents.

2.3. Oxide composition and property weighting

Experimental findings have shown that the oxide composition formed on FeCrAl surfaces is strongly dependent on the oxidation temperature [4]. On the basis of these data, six distinct oxide compositions were selected to reflect different regimes, along with an additional case in which the oxide composition was weighted according to the base alloy composition. These compositions are summarized in Table 2. Cases 1 and 6 were selected as boundary ones, based on the results presented in [4]. Case 1 corresponds to the oxide composition measured after exposure for 30 minutes in an atmosphere at 1 200 °C, whereas case 6 is closely aligned with the oxide composition observed after 12 days of exposure. According to [4], a comparable evolution is also reached at lower temperatures, provided that the exposure period is sufficiently extended. This approach to case definition is therefore consistent with both the temperature- and the time-dependent oxidation behavior. Other cases were defined by alternating the chromium oxide content while simultaneously increasing the aluminum oxide fraction, and thus representing a gradual progression between the two boundary cases.

For each case, the thermophysical properties of FeCrAl oxide were derived by weighting the thermophysical and oxidation properties of Al_2O_3, Cr_2O_3, and Fe_3O_4. This approach ensures that the effective material properties used in the MELCOR simulations reflect the changing contributions of each oxide constituent. Data sets of properties for each respective oxide were retrieved from the NIST JANAF database. Thermal conductivity governs the heat transfer through the formed oxide layer and temperature evolution over time. Specific data were used to define the thermal conductivities of iron and aluminum oxide. For iron oxide, it was assumed that its thermal conductivity would be constant at $3.5\,\mathrm{W\,m^{-1}\,K^{-1}}$ [10]. Chromium oxide thermal conductivity was also assumed constant at $9.99\ \mathrm{W\,m^{-1}\,K^{-1}}$ [11]. Aluminum oxide thermal conductivity was implemented with thermal dependency, given that the formed oxide mixture would be mostly alumina, data were retrieved from [12].

Case	Al_2O_3	Cr_2O_3	Fe_3O_4
Composition 1	0.31278	0.026065	0.182455
Composition 2	0.31278	0.05213	0.15639
Composition 3	0.36491	0.026065	0.130325
Composition 4	0.36491	0.05213	0.10426
Composition 5	0.41704	0.026065	0.078195
Composition 6	0.46917	0.026065	0.026065
Baseline	0.42788	0.069399	0.024023

Table 3. Defined preexponential factors for oxidation kinetics.

The oxidation kinetics were implemented using an Arrhenius correlation 1, which is also used by default in MELCOR calculations.

$$\frac{dW^n}{dt} = k_{p,H_2O} \cdot \exp\left(-\frac{E_a}{RT}\right), \tag{1}$$

where W is the mass of metal oxidized per unit surface area, k_{p,H_2O} is the preexponential factor for water/steam containing environment in ($\mathrm{kg^2\,m^{-4}\,s^{-1}}$), E_a is the activation energy for the reaction to occur ($\mathrm{J\,mol^{-1}\,K^{-1}}$), R is the universal gas constant 8.314 ($\mathrm{J\,mol^{-1}\,K^{-1}}$), T is the temperature of the oxidized surface and n is the reaction order, with $n = 2$ corresponding to the parabolic oxidation rate.

The exact coefficients for the equation for oxidation kinetics for the C35M alloy are not publicly available, and with that given, the kinetics were substituted for the one of Kanthal APMT alloy [2]

$$\frac{dW^2}{dt} = 0.5231 \cdot \exp\left(-\frac{260000}{RT}\right). \tag{2}$$

In this study, the activation energy E_a was kept constant, based on the assumption that diffusion through the alloy governs the oxidation process. The preexponential factor k_{p,H_2O} was scaled according to the mass fraction of each oxide defined by the case, preexponential factors used are summarized in Table 3. This approach reflects the influence of the oxide composition on the oxidation kinetics, while remaining consistent with the MELCOR internal framework for the material definition and the oxidation modeling.

2.4. MELCOR limitations

The current capabilities of MELCOR limit proper modeling of the oxidation of complex alloys such as FeCrAl. Due to FeCrAl oxidation, a layered structure of iron, chromium, and aluminum oxides forms, while also acting as a protective barrier against further oxidation. However, such a mechanism cannot be properly modeled, as MELCOR considers the formation of a single so-called FeCrAl oxide mixture.

The limitation of MELCOR lies in the definition of only three oxidation reactions. For this reason, multiple forms of iron oxide were not considered. It would be appropriate for future studies to also examine separate cases for FeO and Fe_2O_3, as this could lead to different results.

MELCOR framework supports the kinetic model switching for each respective oxide based on the temperature range; however, once the oxide is defined by its thermophysical properties, it remains static. No oxidation kinetics temperature switches were introduced to the model, as the kinetic switch would need to be linked to dynamically evolving oxide properties. In a real environment, the kinetics of formation for each oxide vary over temperatures, and with increasing temperature, the oxide formation growing would be mostly composed of aluminum oxide.

Although the comparative benchmark with other codes has not yet been performed, it would be highly valuable to identify discrepancies arising from code-specific modeling assumptions, and to improve simulation fidelity. The comparison could also help in assessment of sensitivity to input parametrization and oxide material properties definition. Modeling of progression of severe accidents with complex alloys (eg. FeCrAl) as cladding materials could be greatly improved by incorporation of layered oxide modeling support into the code.

2.5. Model limitations

The results are influenced by the relatively coarse nodalization of the core (representation of the entire CORE within a single CVH), which limits the ability to track local phenomena in greater detail. For a more detailed tracking of the local phenomena and degradations such as degree of oxidation, it would be appropriate to perform a sensitivity study, particularly on the time-step length and the nodalization level of detail, as these factors may significantly affect the results and the stability of the calculation with ATF materials.

3. Results and discussion

This section presents a comparative evaluation of the simulation results for six defined FeCrAl oxide compositions, one baseline oxide weighted by the alloy composition, and a Zirconium alloy cladding case.

The results may not necessarily represent definitive physical outcomes tied to the specific composition of a given case, but could instead reflect the sensitivity of

Event	Time to cladding surface reaches 1 204 °C [s]	Time to first cladding failure [s]	Time to support plate failure [s]
Composition 1	1 142 (+0.26 %)	1 740 (+10.83 %)	4 297 (+3.02 %)
Composition 2	1 172 (+2.90 %)	1 935 (+23.25 %)	4 150 (−0.50 %)
Composition 3	1 109 (−2.63 %)	1 815 (+15.61 %)	4 214 (+1.03 %)
Composition 4	1 109 (−2.63 %)	1 860 (+18.47 %)	2 949 (−29.34 %)
Composition 5	1 054 (−7.46 %)	2 105 (+34.08 %)	4 358 (+4.48 %)
Composition 6	1 104 (−3.07 %)	1 880 (+19.75 %)	4 207 (+0.86 %)
Baseline	1 139	1 570	4 171
Zr alloy	1 012 (−11.15 %)	1 840 (+17.20 %)	3 719 (−10.81 %)

TABLE 4. Results comparative matrix with relative error compared to baseline case – events occurring in time.

	Total cumulative hydrogen mass produced [kg]	Total oxidation heat released [GJ]
Composition 1	251.52 (−1.08 %)	14.69 (+1.24 %)
Composition 2	271.14 (+6.64 %)	15.94 (+9.86 %)
Composition 3	252.97 (−0.51 %)	14.29 (−1.52 %)
Composition 4	257.36 (+1.22 %)	15.71 (+8.27 %)
Composition 5	260.82 (+2.58 %)	15.15 (+4.41 %)
Composition 6	282.47 (+11.09 %)	15.93 (+9.79 %)
Baseline	254.26	14.51
Zr alloy	509.11 (+100.19 %)	57.96 (+299.47 %)

TABLE 5. Results comparative matrix with relative error compared to baseline case.

the model and the MELCOR code to input parameters and their implementation.

The comparative matrix Tables 4 and 5) includes key metrics relevant to severe accident progression: reaching of Peak Cladding Temperature (PCT) defined for Zr alloy, first cladding failure, support plate failure, oxidation heat release, and hydrogen production. Relative errors are calculated with respect to the baseline FeCrAl oxide case.

3.1. Temperature evolution and degradation

Figure 3 shows the cladding temperatures in the core node that was first to collapse. The time required for the cladding surface to reach PCT 1 204 °C, the temperature at which Zr alloys start to lose mechanical integrity and the oxidation accelerates. The time to reach this point varied across the compositions by up to 7.5 % from the baseline. Most compositions showed only modest deviations (within ±3 %). These deviations suggest that defined oxide compositions had a limited effect on early heat-up behavior. The exception was Composition 5, which reached 1 204 °C approximately 85 seconds earlier than the baseline, possibly due to a combination of lower oxide thermal conductivity and a residual fraction of iron oxide, and increased oxidation heat feedback from aluminum. Nevertheless, because this outcome is unexpected compared to the other results, it may also reflect a calculation error.

The time to first cladding failure shows more observable differences, with Composition 5 failure delayed by over 500 seconds (+34 %), and Composition 2 by +23 %. These results correlate with a higher aluminum oxide content, which has higher thermal conductivity and chemical stability, thereby improving the protective function of the oxide layer. Notably, the findings indicate that certain oxide compositions can delay cladding failure despite early surface temperature increase.

The time to support plate failure, which reflects the structural failure of the core lower boundary, was relatively consistent across compositions (5 %), with the notable exception of Composition 4. This composition caused the plate to fail approximately 1 200 seconds earlier (−29 %) than the baseline, despite a slower initial heat-up. This behavior is unexpected and suggests that factors beyond simple thermal progression may have influenced the result.

One of the possible explanations would be the earlier onset of localized degradation or a material relocation, potentially caused by chromium and iron oxide content, which have lower thermal conductivities than aluminum oxide. These results would require deeper investigation of the cause, by more finite sensitivity study, but a numerical error in the calculation for this particular case cannot be ruled out.

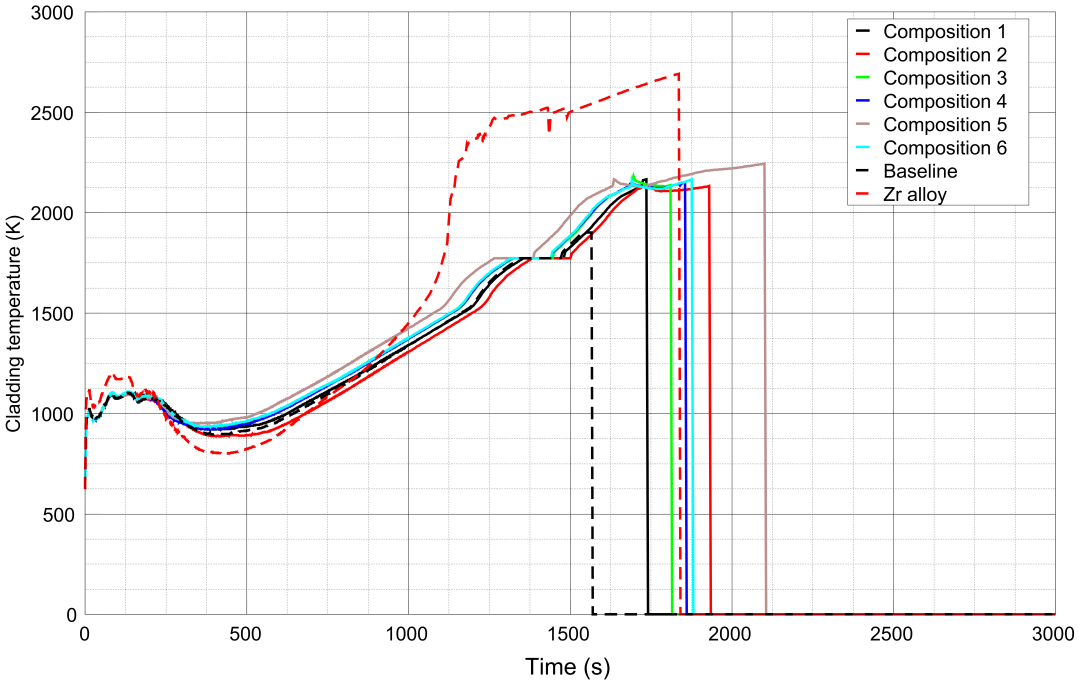

Figure 3. Cladding temperatures in core node that was first to collapse.

3.2. Hydrogen and oxidation heat release

Total hydrogen generation is directly connected with high-temperature oxidation. The plot of total oxidation heat and hydrogen mass released is shown in Figure 4. While most FeCrAl compositions showed deviations within ±3 % of the baseline, Composition 6 produced +11 % more hydrogen mass. This is likely due to a combination of prolonged oxidation period and increased heat released by oxidation itself. The Zr-based cladding case generated twice as much hydrogen as any FeCrAl case, including those with altered oxide compositions, demonstrating the advantage of using ATF claddings in reducing the risk of hydrogen accumulation and potential combustion during severe accidents.

A more substantial variation was observed in oxidation heat released. Composition 6 and Composition 2 released +9.8 % and +9.9 % more oxidation heat than the baseline, respectively. These values are significant when considering that oxidation heat contributes directly to cladding heat-up and core degradation acceleration. This result underlines a critical trade-off in FeCrAl behavior: aluminum-rich compositions enhance protective characteristics, but at the cost of increased heat release. If the heat is not properly dissipated, cladding oxidation tends to accelerate, potentially reducing the time to first deformations and failures. The results reveal a complex relationship between oxide composition, oxidation kinetics, and thermophysical behavior. More Al_2O_3 rich compositions (e.g., Compositions 2, 5 and 6) generally extend the time to cladding failure and delay core melt progression, but this benefit is counterbalanced by increased oxidation heat and hydrogen release. Composition 5, for example, delayed cladding failure by over 500 seconds, but also exhibited one of the shortest times to cladding heat-up and released more energy to the system. Obtained results suggest the presence of an optimal oxide composition range, beyond which further increase in aluminum oxide content becomes detrimental to system-wide behavior due to excessive heat feedback. This nonlinear dependency highlights the importance of considering possible oxide formations and their thermal feedback when evaluating ATF performance under severe accident conditions. These effects cannot be properly modeled and tracked by fixed oxide models weighted to the alloy composition. More advanced modeling frameworks that can reflect oxide evolution dynamically during an accident should be defined, especially in the case of complex multi-elemental alloys.

The Zr alloy case provides a useful benchmark. It reached PCT earlier (−11.2 %), failed sooner, and released almost four times more oxidation heat and about two times more hydrogen mass than the FeCrAl baseline. These results clearly reinforce the enhanced performance of FeCrAl cladding, even under pessimistic assumptions with static oxide definitions.

4. Conclusions

This study investigated the impact of multiple oxide compositions formed on FeCrAl cladding surface under a severe accident phenomena. Defined oxide compositions were evaluated across multiple metrics such as time to failure, oxidation heat released and hydrogen production.

The obtained results indicate that the degradation

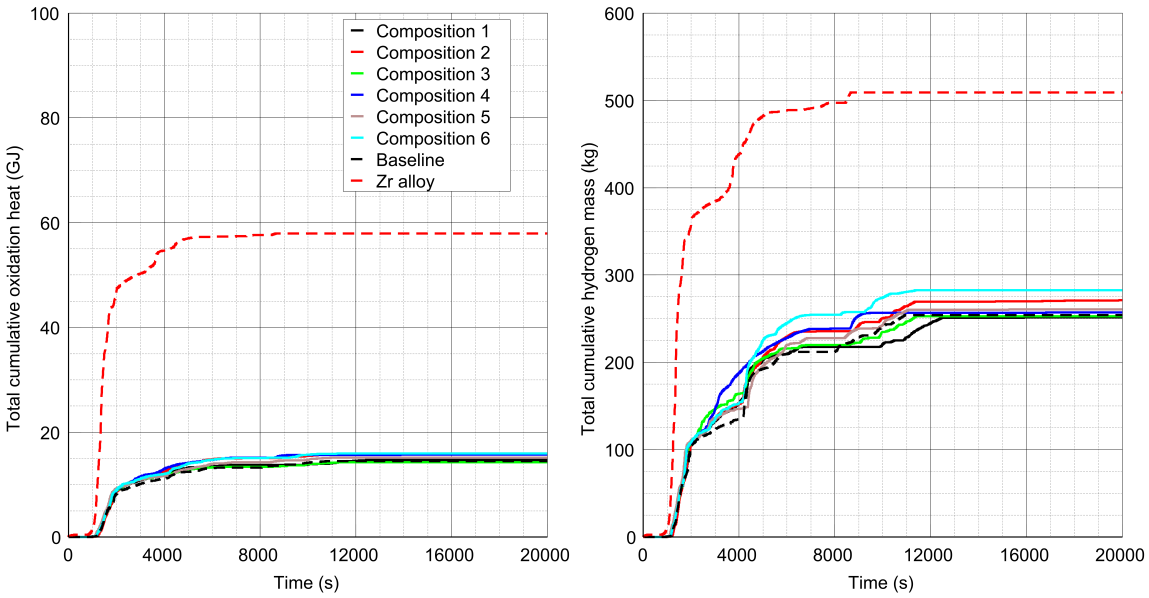

FIGURE 4. Total oxidation heat and cumulative hydrogen mass released.

behavior depends strongly on the oxide composition. Aluminum-rich oxides tend to prolong the time to failure and improve overall resistance, but at the same time they also increase the oxidation heat and the total hydrogen release.

Nevertheless, the results emphasize that the absolute performance of FeCrAl cladding is highly sensitive to its oxidation model. Deviations in data retrieved provide insight that caution should be exercised when interpreting results of severe accident progression with implemented complex alloys without description and incorporation of detailed, temperature-dependent material behavior.

Future work will be aimed at the development of the dynamically evolving oxidation kinetics and corresponding oxide composition models to improve fidelity of accident analyses with ATF cladding materials.

ACKNOWLEDGEMENTS

This research work has been carried out in the Centre for Research and Utilization of Renewable Energy (CVVOZE). Authors gratefully acknowledge financial support from the Technology Agency of the Czech Republic (project No. TN02000012 Centre of Advanced Nuclear Technology II).

REFERENCES

[1] L. I. Albright, D. L. Luxat. Iron-Chromium-Aluminum Accident Tolerant Fuel Concept Source Term Accident Sequence Analysis – High Burnup Fuel Source Term Accident Sequence Analysis Supplement. Technical Report SAND2024-10670, Sandia National Laboratories, Albuquerque, NM, 2024. [2025-06-11]. https://www.nrc.gov/docs/ML2422/ML24229A069.pdf

[2] B. J. Merrill, S. M. Bragg-Sitton, P. W. Humrickhouse. Modification of MELCOR for severe accident analysis of candidate accident tolerant cladding materials. *Nuclear Engineering and Design* **315**:170–178, 2017. https://doi.org/10.1016/j.nucengdes.2017.02.021

[3] P. Mician. Investigation of the hydrogen production by the FeCrAl nuclear fuel cladding using MELCOR 2.2. In *Proceedings II of the 28st Conference STUDENT EEICT 2022: Selected papers*, pp. 220–224. Vysoké učení technické v Brně, Fakulta elektrotechniky a komunikačních technologií, 2022. ISBN 978-80-214-6030-0. https://doi.org/10.13164/eeict.2022.220

[4] C. Badini, F. Laurella. Oxidation of FeCrAl alloy: Influence of temperature and atmosphere on scale growth rate and mechanism. *Surface and coatings technology* **135**(2-3):291–298, 2001. https://doi.org/10.1016/S0257-8972(00)00989-0

[5] M. G. Nathan, K. Terrani, J. Powers, et al. Neutronic analysis of candidate accident-tolerant cladding concepts in pressurized water reactors. *Annals of Nuclear Energy* **75**:703–712, 2015. https://doi.org/10.1016/j.anucene.2014.09.005

[6] R. B. Rebak. Improved and innovative accident-tolerant nuclear fuel materials considered for retrofitting light water reactors – A review. *Corrosion and Materials Degradation* **4**(3):466–487, 2023. https://doi.org/10.3390/cmd4030024

[7] *APR1400 Design Control Document*. Revision 3. Korea Electric Power Corporation and Korea Hydro and Nuclear Power CO., LTD, 2018. [2025-06-12]. https://www.nrc.gov/reactors/new-reactors/large-lwr/design-cert/apr1400/dcd

[8] K. G. Field, M. A. Snead, Y. Yamamoto, K. A. Terrani. Handbook on the Material Properties of FeCrAl Alloys for Nuclear Power Production Applications (FY18 Version: Revision 1). Tech. rep., Oak Ridge National Laboratory (ORNL), Oak Ridge, TN (United States), 2018. https://doi.org/10.2172/1474581

[9] Kanthal AB. Kanthal® APMT Tube Datasheet, 2024. [2025-06-14]. https://www.kanthal.com/en/products/material-datasheets/tube/kanthal-apmt/

[10] M. Li, M. Akoshima, R. Endo, et al. Thermal diffusivity and conductivity of Fe_3O_4 scale provided by oxidation of iron. *ISIJ International* **62**(1):275–277, 2022. https://doi.org/10.2355/isijinternational.ISIJINT-2021-326

[11] J. F. Shackelford, W. Alexander. *Materials Science and Engineering Handbook*. CRC Press LLC, 3rd edn., 2001. https://doi.org/10.1201/9781420038408

[12] R. Lo Frano, D. Aquaro, L. Scaletti, N. Olivi. Characterization of the thermal conductivity for ceramic pebble beds. *Journal of Physics: Conference Series* **655**(1):012057, 2015. 33rd UIT Heat Transfer Conference, 22–24 June 2015, L'Aquila, Italy. https://doi.org/10.1088/1742-6596/655/1/012057